

Process Design of Micro-Arc Oxidation Coatings Based on Magnesium Lithium Alloy and Their Characteristics

Shuo-Jen Lee¹, Le-Hung-Toan Do^{1,*}, Jeou-Long Lee², Huan-Chih Peng¹

¹ Department of Mechanical Engineering, Yuan Ze University, Chung-Li, Taiwan 32003, R.O.C.

² Department of Chemical and Material Engineering, Lunghwa University of Science and Technology, Guishan, Taoyuan County 33306, Taiwan, R.O.C.

*E-mail: toandlh@gmail.com, s1028705@mail.yzu.edu.tw

Received: 6 September 2017 / Accepted: 20 October 2017 / Published: 12 November 2017

Micro-arc oxidation processes have several advantages and a high ability to be applied for corrosion protection to magnesium lithium alloys. The present study investigates the process design of micro-arc oxidation coated on an LZ91 magnesium alloy in an alkaline electrolyte. Coating thickness (t_a), corrosion resistance (R_p) and coating uniformity (t_u) are utilized as indices for surface characteristics. The salient effects of the three key process parameters: current density, coating time and electrical frequency, on surface characteristics are identified with the use of the Taguchi method and optimal analysis. The relationship between the coating thickness and the uniformity of the coating is established to control the MAO coating process. The major factor affecting the corrosion resistance of the coatings is the current density. The results show that the predicted values for coating thickness (t_a) and corrosion resistance (R_p) are in close agreement with confirmation experimental results. Therefore, the surface characteristics of MAO coated LZ91 could be designed through the Taguchi design of experimentation and related optimal analyses.

Keywords: micro-arc oxidation (MAO), Taguchi method, coating thickness, corrosion resistance

1. INTRODUCTION

Mg–Li alloys with a low density, high recyclable ability, high strength–to-weight ratio, high damping capacity, high specific stiffness and good machining properties are applied in numerous industries, such as in the automotive industry, consumer electronics and aerospace [1-3]. In spite of numerous excellent properties, the use of magnesium lithium alloys has been restricted because of some major limitations [4]. Magnesium corrodes rapidly in aggressive environments and does not form protective oxide film on their surfaces, which causes them to lose their mechanical integrity and creates an unprepossessing appearance [5]. In addition, alloying with the high chemical reactivity of

lithium also makes this alloy extremely poor for corrosion and wear resistance. The dual phase structure of Mg-Li (5 to 11.5% Li) alloys enhances the deformability and ductility of the binary Mg-Li alloys due to the presence of the β phase [6, 7]. However, the Body Centered Cubic (BCC) structure of the β phase shows better mechanical properties but is worse in corrosion resistance [8, 9].

Hence, many surface treatment technologies have been investigated to improve corrosion resistance for magnesium-lithium alloys, such as electrodeposition, chemical conversion plating, organic coating, vapor-phase processes, and micro-arc oxidation [10-13]. As a relatively new and popular technique for the surface treatment of magnesium alloys, the micro-arc oxidation (MAO) method shows numerous advantages and a high ability to be applied to magnesium lithium alloys. The protective layers are produced on a magnesium-lithium alloy surface by the action of electricity in a convenient electrolyte [14-16]. The interactions of various microdistrict processes under discharge channels result in the production of a compact, thick, hard layer, which often has attractive abrasion and corrosion resistances [17]. The properties of MAO coating mainly depend on the chemical compositions of the magnesium alloys, electrolyte composition current regimes, applied voltage/current density, electrical frequency, duty cycle, processing time, etc. [18-20]. The influence of electrolytes and additives on the characteristics of coatings fabricated on magnesium lithium alloys by the MAO process has previously been studied. Our previous study indicated that the corrosion resistance of magnesium lithium alloys was significantly improved after being treated by the MAO technique [21]. Many researchers have studied the effects of current density on the characteristics of MAO coated magnesium alloys [17, 22-24]. In general, at a low current density, the MAO coating is thin, smooth and uniform. With the increase in current density beyond a critical value, the porosity of coating increases, which results in rough and non-uniform coatings [25]. The electrical frequency is also an important factor that influences the properties of MAO coatings. An increase in electrical frequency causes a shorter pulse time and lower energy per pulse. A higher electrical frequency enables the formation of a compact coating with a smooth surface finish and decreases in porosity [26]. Hwang *et al.* [27] also reported that the volume fraction of MgO in the coating increased with the increase in electrical frequency. The corrosion resistance of the MAO coatings is significantly improved because of the formation of a compact and dense coating with a higher volume fraction of MgO. According to Gu *et al.* [28], the processing time of MAO affects the coating thickness and corrosion behavior. A compact, smooth and uniform morphology with lower porosity can be produced at an optimized oxidation time.

Recently, the characteristics of MAO coating fabricated on magnesium lithium alloys have been investigated [8, 21, 29, 30]. However, few studies have been carried out to design and optimize the MAO processing parameters for fabrication of quality coatings. In this study, the micro-arc oxidation process is optimized by the Taguchi method to design a coating thickness with good anti-corrosion performance on magnesium lithium alloy. The coating thickness and corrosion resistance of MAO coatings depend on several electric parameters such as current density, electrical frequency and coating time. The results of the factor response analysis were used to derive optimal levels. The optimum results are further verified by conducting confirmation experiments.

2. EXPERIMENTAL INVESTIGATION AND METHOD

2.1 Coating characterization

Three indices, including coating thickness (t_a), corrosion resistance (R_p) and the uniformity of the thickest coating (t_u), are utilized for surface characteristics. The thickness of the MAO coatings (t) was obtained by averaging the nine measurements (t_a) and its standard deviations (σ) on the surface using a Fischer dualscope MP20 for non-ferrous materials. The measurement was in accordance with the Eddy current principle and used to measure the thickness of the nonconductive coating on non-ferromagnetic conductive substrate.

$$t = t_a \pm \sigma \quad (1)$$

For corrosion resistance (R_p) evaluation of the coatings, potentiodynamic polarization was performed on Solartron 1285. Potentiodynamic polarization measurements were conducted in a 3.5 wt% NaCl solution at room temperature using a conventional three-electrode cell with a Mg–Li alloy or coated alloy with an exposed area of 1 cm² as the working electrode, a Silver Chloride Electrode (Ag/AgCl/Sat. KCl) as the reference electrode and a platinum plate as the counter electrode. Potentiodynamic polarization tests were conducted from -1.8 V to -1.2 V at a scanning rate of 1 mV/s. The corrosion current density i_{corr} , corrosion potential E_{corr} and the constants of the anodic (β_a) and cathodic (β_c) Tafel slopes were extracted directly from the potentiodynamic polarization curves to evaluate the corrosion protective properties of MAO coatings. The polarization resistance (R_p) was obtained by using the Stern-Geary Equation (2) [31]:

$$R_p = \frac{\beta_a \beta_c}{2.3 i_{\text{corr}} (\beta_a + \beta_c)} \quad (2)$$

Equation (3) is used to present the coating thickness with high uniformity. The thickest coating uniformity (t_u) is designed by combining the responses of the coating thickness (t_a) and its standard deviations (σ) for the nine-point measurements.

$$t_u = \frac{t_a}{10 \times \sigma} \quad (3)$$

The surface and cross-sectional morphologies of the optimized MAO coatings was assessed using a scanning electron microscope (SEM) (FEI Nova NanoSEM 230).

2.2 Taguchi method of designing experiments

The Taguchi method is a widely used technique used for optimizing or design a process using multiple input parameters. It is an experiment that allows researchers to design a product or process that functions more consistently in the operating environment. It recognizes that not all factors that cause variability can be controlled. These uncontrollable factors are called noise factors. The method identifies controllable factors that minimize the effect of the noise factors. Taguchi developed a special design of orthogonal arrays to study the entire parameter space with only a small number of experiments. As a result, the Taguchi method provides a simple, efficient and systematic approach to determine optimum conditions.

The experimental results are then transformed into a signal-to-noise (S/N) ratio. This method uses the S/N ratio as a measure of quality characteristics deviating from or nearing the desired values

and indicates the degree of predictable performance by the occurrence of noise factors. Depending on the criteria used for optimization of the quality characteristics, the S/N ratio can be classified as the “larger is better”, the “nominal is best” or the “lower is better”.

The process factors affecting thickness and corrosion of the micro-arc oxidation coating are current density, coating time and electrical frequency. The three three-level factors are studied to find their optimum levels to produce the micro-arc oxidation coating of magnesium lithium alloy with the greatest thickness and corrosion resistance. Prior to conducting the designed experiments, a few samples were coated under several extreme conditions and tested to ensure that the selected factor levels were functional and feasible. **Table 1** summarizes the factors and levels of the experimental design.

Table 1. Factors and levels for the L9 (3^3) Taguchi experimental design.

Factors	Unit	Factor levels		
		1	2	3
(A) Current density	(A/dm ²)	3	4	5
(B) Coating time	(Minutes)	5	10	15
(C) Electrical frequency	(Hz)	500	1000	2000

According to Taguchi’s design of experiments, an L9 orthogonal array including the three factors and three levels was selected. The experimental design matrix – L9 (3^3) is described in **Table 2**. With the selection of an L9 orthogonal array, the number of experiments required can be reduced to 9. Hence, nine experiments are conducted to study the main effects whereas full factorial experimentation would require 27 experiments. The experiments were randomly run during the same shift on the same day to eliminate the effect of uncontrollable factors.

Table 2. Experimental design matrix of L9 (3^3) orthogonal array.

Factors	Unit	Experiment number								
		1	2	3	4	5	6	7	8	9
(A) Current density	(A/dm ²)	3	3	3	4	4	4	5	5	5
(B) Coating time	(min)	5	10	15	5	10	15	5	10	15
(C) Electrical frequency	(Hz)	500	1000	2000	1000	2000	500	2000	500	1000

2.3 Preparation of micro-arc oxidation coatings

Rectangular coupons of LZ91 alloy (9 wt% Li, 1 wt% Zn and Mg balance) with the dimensions of 33 mm × 75 mm × 5 mm were used as the specimens for MAO coating processes in this study. All

samples were prepared from the area of a cast ingot in order to minimize the differences in microstructure and composition. Prior to the MAO process, the Mg-Li alloy specimens were ground and polished using a 1200 mesh abrasive paper, cleaned in acetone and dried in cool air.

During the MAO process LZ91 alloy substrates were used as the anode, and a stainless steel bath, with the size of 150 mm × 150 mm × 150 mm, was used as the cathode. The temperature of the electrolyte was kept at 20°C by a cooling system. The MAO coatings were conducted in the alkaline silicate electrolyte studied previously [21]. The treatment parameters are shown in Table 2. After the MAO treatment, the coated samples were rinsed thoroughly with distilled water and dried in hot air.

3. RESULTS AND DISCUSSION

Table 3 shows the responses of variables as coating thickness (t), corrosion resistance (R_p) and coating uniformity (t_u) results for Taguchi’s L9 orthogonal array. The nine experiments from L9 Taguchi’s method of experimental design were conducted three times to ensure the repeatability of experimental data for signal-to-noise analysis. The trial result data was transformed into a signal-to-noise (S/N) ratio for the response to evaluate the coating quality in the designed optimum process parameter analysis. Depending on the criteria used for the designed optimization of the quality characteristics, the S/N ratio can be classified as the “larger is better”, the “nominal is best” and the “lower is better”. In this study, the coating thickness, corrosion and thickest coating uniformity were intended to be maximized. Therefore, the larger is the better S/N ratio was selected. The formula used for calculating the S/N ratio is given below.

Larger is better:

$$S/N = S/N = -10 * \log(\Sigma(1/Y^2)/n) \tag{4}$$

Where n is the repetition number of each experiment under the same condition for design parameters, and Y is the observed response value. The Minitab is used to calculate and plot the mean S/N ratios at each level for various factors, the optimal condition is the largest S/N ratio value.

Table 3. Responses of coating thickness (t), corrosion resistance (R_p) and the thickest coating uniformity (t_u) of MAO coatings.

Exp no.	Coating thickness, t (µm)			Corrosion resistance, R _p (kΩ.cm ²)			Thickest coating uniformity, t _u		
	Test 1	Test 2	Test 3	Test 1	Test 2	Test 3	Test 1	Test 2	Test 3
1	6.2 ± 0.54	5.3± 0.53	6.0 ± 0.68	43.42	68.38	44.13	1.15	1.00	0.88
2	14.1 ± 0.60	10.7± 0.66	12.8 ± 0.52	296.17	277.36	243.78	2.35	1.62	2.46
3	16.4 ± 0.67	12.9± 0.33	13.5 ± 0.89	213.00	244.34	253.42	2.45	3.91	1.52
4	8.8 ± 0.52	8.7± 0.54	8.9 ± 0.66	173.02	162.91	148.70	1.69	1.61	1.35
5	16.6 ± 0.64	14.2± 0.49	18.7 ± 0.74	70.30	52.48	54.04	2.59	2.90	2.53
6	26.1 ± 1.30	23.7± 0.82	26.1 ± 1.10	145.71	110.01	159.97	2.01	2.89	2.37
7	11.3 ± 0.69	10.4± 0.67	10.4 ± 0.60	162.95	127.67	135.62	1.64	1.55	1.73
8	23.5 ± 0.93	22.7± 0.96	21.3 ± 1.00	103.75	133.87	105.09	2.53	2.36	2.13
9	23.9 ± 1.20	26.7± 2.00	26.2 ± 1.60	48.74	75.98	50.56	1.99	1.34	1.64

3.1 Coating thickness

3.1.1 Determination of optimal coating thickness

The results of coating thickness measurements conducted according to Taguchi’s orthogonal array for various combinations of parameters are analyzed by the statistical software package Minitab. The experimental results were transformed into the “larger is better” S/N ratio, since the goal was to find the thickest coating. The S/N ratio values for all responses are presented in Table 4 and Figure 1.

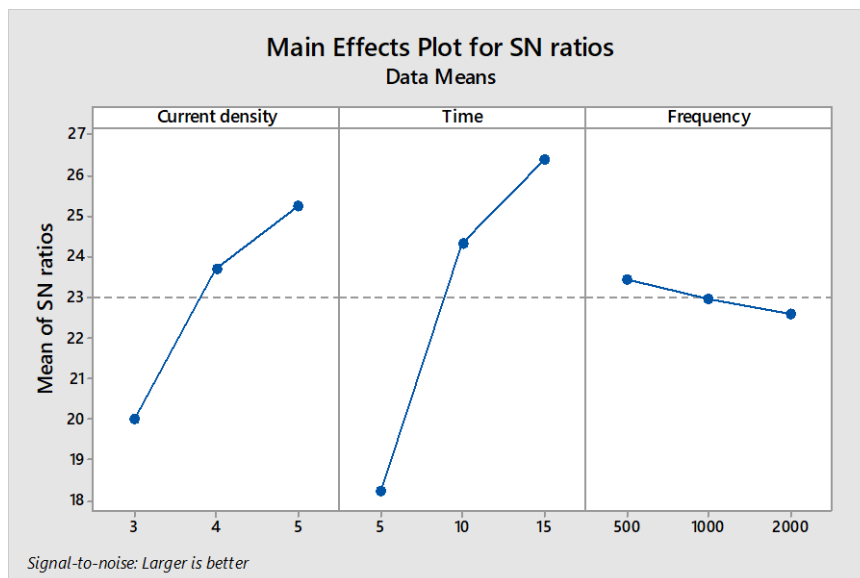


Figure 1. Main effects plot for S/N ratios versus factor levels of coating thickness.

Table 4. Response for S/N ratios _ Larger is better for coating thickness.

Level	Factor		
	Current density (A/dm ²)	Coating time (min)	Electrical frequency (Hz)
1	20.00	18.24	23.44
2	23.70	24.33	22.94
3	25.24	26.37	22.57
Delta	5.24	8.13	0.87
Rank	2	1	3

The mean S/N ratio increases linearly with the current density and time. According to Gu *et al.* [28], the coating thickness is a function of the current density and coating time. Increase in current density generally enhances the growth rate, leads to increase the thickness of the MAO coating. X. Lu *et al.* [32] also reported that the thickness of the MAO coating is influenced significantly by the electrical frequency; the lower electrical frequency produces thicker MAO coatings. Results from this study show that the process parameters for the optimum coating thickness are obtained as the current

density at Level 3 (5 A/dm²), the coating time at Level 3 (15 min) and the electrical frequency at Level 1 (500 Hz). The difference between the minimum and maximum values of the S/N ratio is shown in Table 4. It is clear that the sequence of the factors with respect to increasing the influence of coating thickness is electrical frequency < current density < coating time. Coating time is the factor that has the highest difference value ($\Delta = 8.13$). According to the Taguchi prediction method, a greater difference between the minimum and maximum values of the S/N ratio will have a more significant effect on the coating thickness. By using Minitab, the highest estimated average coating thickness was found to be 27.6 μm .

3.1.2 Confirmation run for the optimal coating thickness

Confirmation runs were performed with settings at: current density at Level 3 (5 A/dm²), time at Level 3 (15 min) and electrical frequency at Level 1 (500 Hz). Table 5 shows the prediction and confirmation run results for MAO coated on LZ91 substrate under 5A/dm² for 15 min and 500 Hz. The thickness coated on LZ91 substrate from the optimized parameters is 27.5 ± 1.80 (μm). The result of the confirmation run is consistent with the expected value (27.6 μm). The difference with the Taguchi prediction method is 0.1 μm in confirming the success of statistical analysis. By using a high current density, long process time and low electrical frequency, the thickest coating can be formed. However, the surface is rough ($R_a \sim 1.93$ μm and $R_z \sim 14.83$ μm) and non-uniform because the sparking discharge is very strong during the MAO coating process. As show in Table 5, the corrosion resistance of the thickest coating is 81.66 $\text{k}\Omega\cdot\text{cm}^2$, which is consistent with the Taguchi prediction value (76.67 $\text{k}\Omega\cdot\text{cm}^2$).

Table 5. The results of prediction and confirmation run of MAO treated LZ91 at 5 A/dm², 15 min, 500 Hz.

	Coating thickness, t_a (μm)	Corrosion resistance, R_p ($\text{k}\Omega\cdot\text{cm}^2$)	Thickest coating uniformity, t_u
Predicted	27.6	76.67	2.02
Confirmation	27.5 ± 1.80	81.66	1.52

The morphologies of the surface and cross-sectional views of the MAO coating specimen are illustrated in Figure 2. It can be seen that the ceramic coatings fabricated by the MAO process have a porous microstructure and some volcano top-like pores distributed disorderly on the coatings' surfaces, and the size of the pores is obviously affected by the electrical parameters. The morphology of coatings fabricated under optimal parameters to get the thickest coating exhibits relatively coarse pores. According to Qiu et al. [33] increase in current density leads to increase in discharge energy and enlarge the pore sizes. The micro cracks also appeared on the coating due to the thermal stress and high pressure under the high reaction temperature. Moreover, with increase in processing time, the intensity of the spark discharge is increased and the number of spark discharge is decreased. The

higher energy input during the MAO process with the increase in processing time can create a thicker coating. This indicates that the high current density at low electrical frequency will generate a discharge spark during the micro-arc oxidation process resulting in the formation of bigger pores and micro-cracks on the coating.

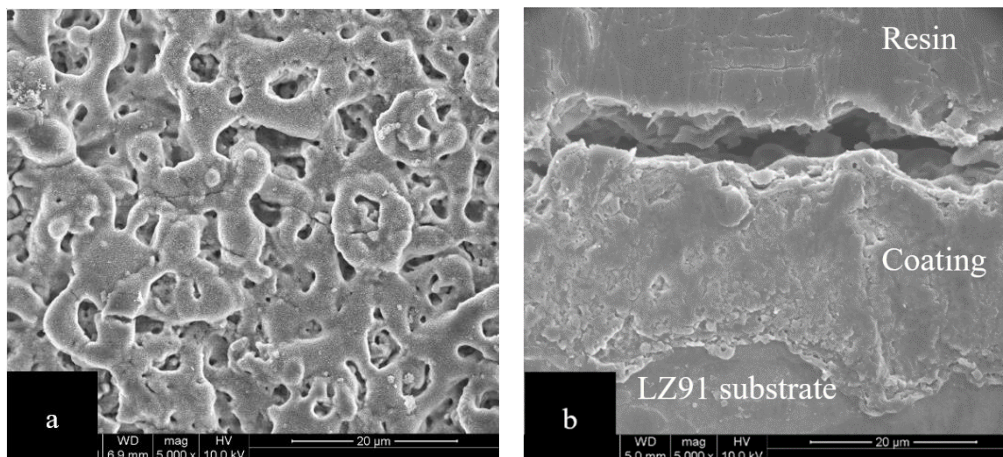


Figure 2. (a) Top morphology and (b) cross-sectional images of MAO coatings performed under optimized coating thickness parameters (5 A/dm^2 , 15 min, 500 Hz).

3.2 Corrosion resistance

3.2.1 Determination of optimal level of corrosion resistance

The signal-to-noise ratio of “Larger is Better” is selected for corrosion resistance, since the goal is to find higher corrosion resistance values. Hence, the signal-to-noise expression from Equation (4) was used for analysis. The S/N ratio values for all responses are presented in Table 6 and Figure 3. By examining the main effects plot for S/N ratios shown in Table 6 and Figure 3 we can conclude that for corrosion resistance, the factor with the largest effect appears to be current density ($\Delta = 3.69$) followed by electrical frequency ($\Delta = 3.44$). The S/N ratio decreases with the increase in current density. The corrosion resistance of MAO coatings depends on the surface morphology, porosity and coating thickness. According to Ma *et al.* [34], corrosion resistance decreases with the increase in current density. At a high current density, the discharge spark becomes intense, resulting in the formation of a rough, porous and non-uniform coating. However, at a low current density, the sparking is uniformly distributed on the surface leading to the fabrication of dense, fine micropores and a uniform coating.

The response of the S/N ratio to the electrical frequency reaches a value of 42.52 at an electrical frequency of 1000 Hz. After that, the mean S/N ratio decreases with the increase in electrical frequency. An increase in electrical frequency results in the fabrication of a compact and dense coating. This provides a significant improvement in corrosion resistance for MAO coatings. The variation in discharge characteristics is considered responsible for the observed difference in the extent of porosity and cracks as a function of electrical frequency. Moreover, the thickness varying with

electrical frequency plays an important role in improving the corrosion resistance of the coatings. The process time shows the lowest effect on the corrosion resistance of MAO coatings. Gu *et al.* [28] reported that the coating time has little effect on the corrosion resistance of an MAO coating. A high corrosion resistance coating can be produced at an optimum coating time due to the compact, smooth and uniform morphology produced with low porosity. The optimum process parameters for corrosion resistance are obtained as the current density at Level 1 (3 A/dm²), time at Level 2 (10 min) and electrical frequency at Level 2 (1000 Hz). Under optimum conditions, the expected value of corrosion resistance predicted by the Taguchi method is 225.31 kΩ.cm².

Table 6. Response for S/N ratios _ Larger is better for corrosion resistance.

Level	Factor		
	Current density (A/dm ²)	Coating time (min)	Electrical frequency (Hz)
1	43.27	40.27	39.08
2	40.60	41.60	42.52
3	39.58	41.58	41.84
Delta	3.69	1.33	3.44
Rank	1	3	2

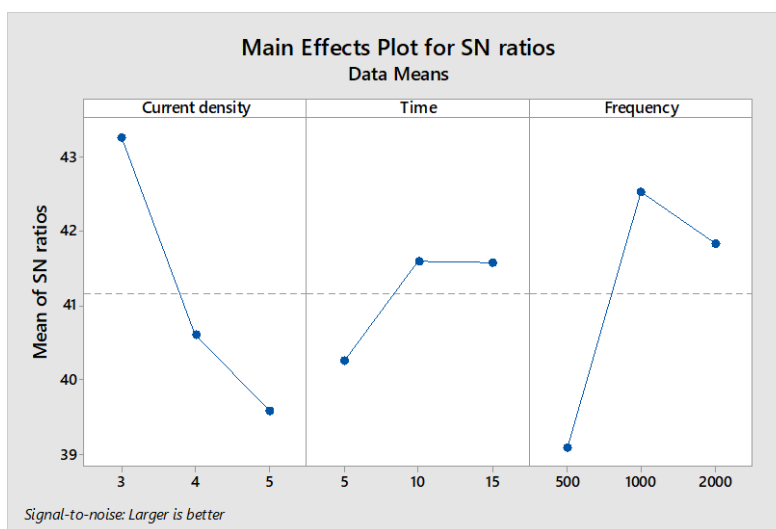


Figure 3. Main effects plot for S/N ratios versus factor levels of corrosion resistance.

3.2.2 Confirmation runs for the optimal corrosion resistance

Confirmation runs were performed by setting the experimental conditions for the three factors as: current density at Level 1 (3 A/dm²), time at Level 2 (10 min) and electrical frequency at Level 2

(1000 Hz). Table 7 shows the prediction and confirmation run results for MAO coated on LZ91 substrate under optimized conditions. The thickness of the highest corrosion resistance coating is $12.3 \pm 0.68 \mu\text{m}$, which is consistent with the Taguchi prediction value ($12.1 \mu\text{m}$), and the coating surface is smooth and uniform with $R_a \sim 0.63 \mu\text{m}$ and $R_z \sim 4.99 \mu\text{m}$.

Table 7. The results of prediction and confirmation run of MAO at 3 A/dm^2 , 10 min, 1000 Hz.

	Coating thickness, t_a (μm)	Corrosion resistance, R_p ($\text{k}\Omega\cdot\text{cm}^2$)	Thickest coating uniformity, t_u
Predicted	12.1	225.31	2.08
Confirmation	12.3 ± 0.68	256.85	1.81

The top surface morphologies and the cross-sectional views of the MAO coating specimen are illustrated in Figure 4. It is observed that the coating exhibited a porous surface morphology with lots of volcano top-like pores. According to Liu et al. [35], the porosity of MAO coating is due to the non-uniform growing pattern and trapping of oxygen bubbles in the coating growth process. The coating formed under optimal parameters of corrosion resistance exhibits a uniform surface morphology with small discharge pores. It can be seen from the cross-sectional image (Figure 4 (b)) that the coating is dense and uniform.

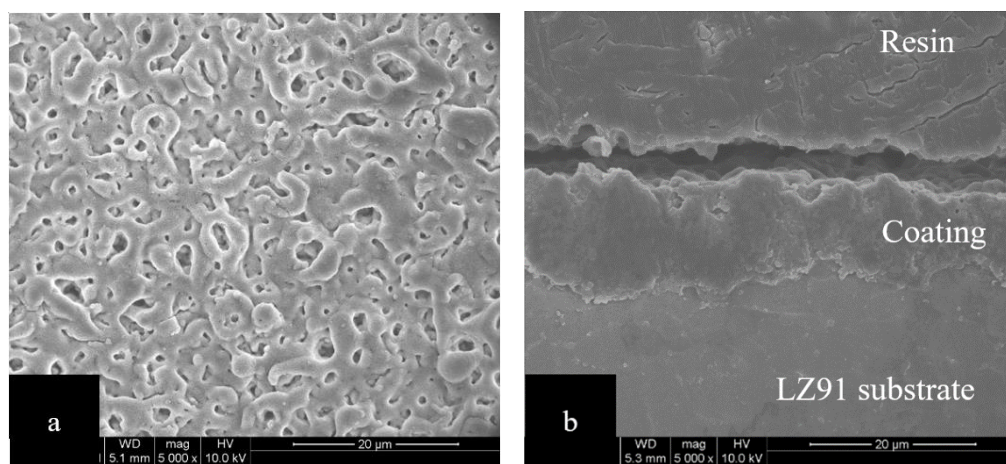


Figure 4. (a) Top morphology and (b) cross-sectional images of MAO coatings performed under optimized corrosion resistance parameters (3 A/dm^2 , 10 min, 1000 Hz).

Figure 5 and Table 8 show potentiodynamic polarization curves and their electrochemical parameters of the untreated and MAO treated LZ91 sample from the confirmation run at 3 A/dm^2 , 10 min and 1000 Hz. In general, a better corrosion behavior can be identified by high corrosion potential, low current density and high corrosion resistance [36]. It can be seen from Table 8 that the corrosion potential of the optimized coating is more positive (-1.53 V) than that of the untreated LZ91 substrate (-1.61 V), and the corrosion current density of the coating ($6.78 \times 10^{-8} \text{ A/cm}^2$) is lower than that of the untreated LZ91 substrate ($9.98 \times 10^{-6} \text{ A/cm}^2$). Thus, the coating could be corroded only at a relatively

higher potential and with a lower corrosion rate than the untreated LZ91 substrate. Based on the approximately linear polarization behavior, the polarization (R_p) were determined by the equation (2). The corrosion resistance of the optimized coating is $256.85 \text{ k}\Omega\cdot\text{cm}^2$, which is the highest value obtained in the present study and close to the predicted value ($225.31 \text{ k}\Omega\cdot\text{cm}^2$). The corrosion resistance of the optimized coating is about 145 times higher than that of the untreated substrate.

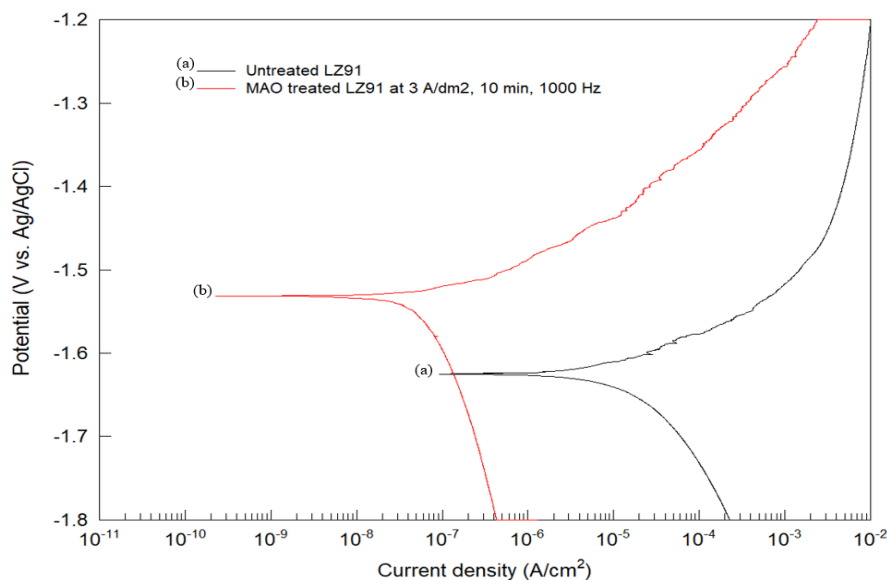


Figure 5. Polarization curves of untreated and MAO treated LZ91 at 3 A/dm^2 , 10 min and 1000 Hz.

Table 8. Electrochemical corrosion properties of untreated and MAO treated LZ91 at 3 A/dm^2 , 10 min and 1000 Hz.

Samples	β_a (mV/decade)	β_c (mV/decade)	i_{corr} (A/cm^2)	E_{corr} (V vs. Ag/AgCl)	R_p ($\text{k}\Omega\cdot\text{cm}^2$)
Untreated LZ91	59.7	126.6	9.98×10^{-6}	-1.61	1.77
MAO treated LZ91	52.0	173.7	6.78×10^{-8}	-1.53	256.85

3.3 The thickest coating uniformity

3.3.1 Determination of the optimal thickest coating uniformity

The signal-to-noise ratio of “Larger is Better” is selected for the combined thickness and coating uniformity, since the goal is to find uniform and thicker coating values. Hence, the expression for the signal-to-noise ratio for “larger is better” was used for analysis. The S/N ratio values for all responses are presented in Table 9 and Figure 6. By examining the main effects plot for the S/N ratio shown in Figure 6 we can conclude that for combined thickness and coating uniformity, the factors with the greatest effect appear to be coating time followed by current density. Accordingly, the result shows that the second level of current density, the second level of coating time and the third level of electrical frequency are higher. Therefore, the optimum process parameters for the combined thickness

and coating uniformity are obtained as the current density at 4 A/dm², coating time at 10 min and electrical frequency at 2000 Hz. Growth rate of coating increases linearly with increase in applied current density. However, further increase has adverse impact impacts on coating uniformity [37]. Gu et al. [28] studied the effect of processing time on the thickness of MAO coating on magnesium alloy, and reported that the excessively long processing duration decreased the thickness and uniformity of coating. At high electrical frequency, the number of discharge channels are increased and the pores size is reduced. The coatings seem smooth and with a little disfigurement [38]. Hence, a longer coating time with higher current density can produce a thick coating while the high electrical frequency helps the coating to be smoother and more uniform.

Table 9. Response for S/N ratios _ Larger is better for thickest coating uniformity.

Level	Factor		
	Current density (A/dm ²)	Coating time (min)	Electrical frequency (Hz)
1	4.21	2.63	4.89
2	6.53	7.32	4.62
3	5.21	5.99	6.43
Delta	2.32	4.69	1.81
Rank	2	1	3

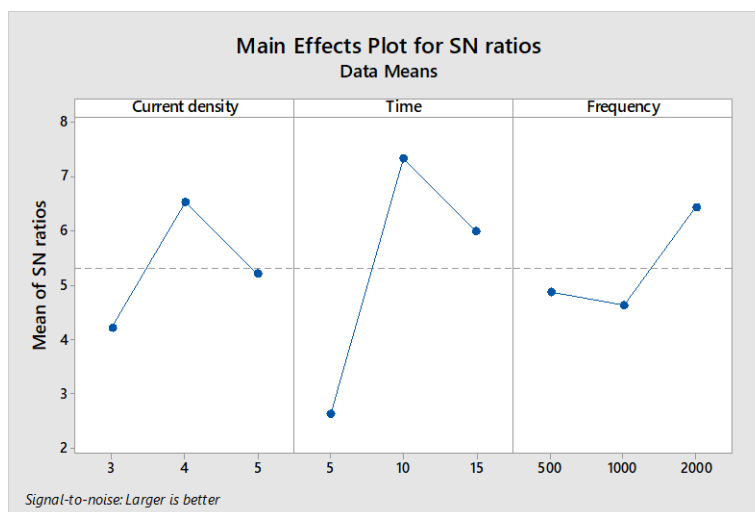


Figure 6. Main effects plot for S/N ratios versus factor levels of thickest coating uniformity.

3.3.2 Confirmation runs for the optimal thickest coating uniformity

Confirmation runs were performed by setting the experimental conditions for the three factors as: current density at Level 2 (4 A/dm²), time at Level 2 (10 min) and electrical frequency at Level 3 (2000 Hz). The thickness of the coating is 16.8 μm while the standard deviation of the 9 points

measurements is 0.56 μm . From these results, the t_u value is 3, which is close to the predicted value (2.90).

The top surface morphologies and the cross-sectional views of the MAO coating produced under conditions of 4 A/dm^2 , 10 min and 2000 Hz are shown in Figure 7. Typical small porous microstructures and a uniform morphology are observed in all the coatings. It can be seen from the cross-sectional image (Figure 7 (b)) that the coating is dense and uniform. The coating thickness (approximately 16 μm) is corroborated with results obtained from the Eddy current probe thickness measurement.

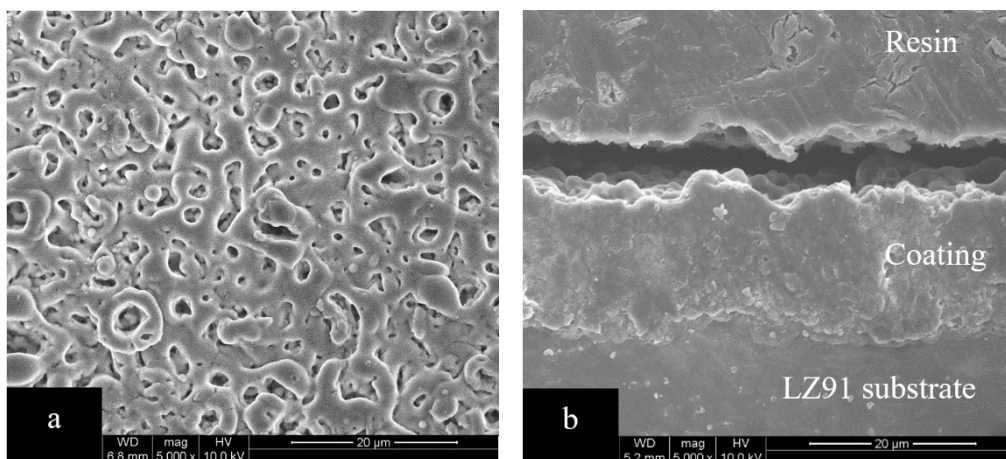


Figure 7. (a) Top morphology and (b) cross-sectional images of MAO coatings performed under optimized thickest coating uniformity parameters (4 A/dm^2 , 10 min, 2000 Hz).

Table 10 shows the prediction and confirmation run results of MAO coated on LZ91 substrate produced under conditions of 4 A/dm^2 , 10 min and 2000 Hz. The corrosion resistance of the thickest uniform coating is 89.96 $\text{k}\Omega\cdot\text{cm}^2$, which is about 46 times higher than that of the untreated LZ91 substrate.

Table 10. The results of prediction and confirmation run of MAO treated LZ91 at 4 A/dm^2 , 10 min, 2000 Hz.

	Coating thickness, t_a (μm)	Corrosion resistance, R_p ($\text{k}\Omega\cdot\text{cm}^2$)	Thickest coating uniformity, t_u
Predicted	16.3	139.73	2.90
Confirmation	16.8 \pm 0.56	89.96	3.00

4. CONCLUSIONS

The method of experimental design has been used for designing, optimizing and determining the effects of current density, coating time and electrical frequency on the electrolytic plasma

oxidation process for the fabrication of an oxide coating for the corrosion protection of a magnesium-lithium (LZ91) alloy.

The MAO process time is found to be the major factor affecting the coating thickness. The electrical frequency has little effect on the thickness of coating. The optimized processing parameters used to form the thickest coating are 5 A/dm² for current density, 15 min for process time and 500 Hz for electrical frequency. The optimal coating thickness is 27.5 μm, which is close to the Taguchi prediction value (27.6 μm). However, the surface is rough and non-uniform due to the strong discharge.

In order to form the best corrosion resistance coating, the optimized processing parameters are set at 3 A/dm² for current density, 10 min for treatment time and 1000 Hz for electrical frequency. The current density is found to be the major factor affecting the coating thickness. The thickness of the coating is about 12.3 ± 0.68 μm and is consistent with the predicted value (12.1 μm). The coating fabricated under these conditions is smooth and uniform. The corrosion resistance of the optimized coating is more than 145 times better than that of the untreated LZ91 alloy substrate.

The thickest coating's uniformity is analyzed to control the thickness and ensure its uniformity. The thickest coating uniformity is produced at 4A/dm², 10 min and 2000 Hz. The coating thickness is 16.8 μm while the standard deviation of 9 points measurements is 0.56 μm, and the t_u is calculated at about 3, which is consistent with the Taguchi prediction value. The corrosion resistance of the surface is improved compared with untreated LZ91 alloy substrate.

The present approach indicates that the application of Taguchi's experimental design was successful as an efficient method to optimize and design the desired coating thickness, corrosion resistance and the thickest coating uniformity. Predicted values using the Mathematical model were in close agreement with the results obtained in confirmation runs.

ACKNOWLEDGEMENTS

This work was accomplished with much needed support and the authors would like to thank for the financial support by Ministry of Science and Technology of R.O.C. and AmLi Co., Ltd. through the grant MOST 106-2622-E-155-001-CC2.

References

1. C. Liu, J. Liang, J. Zhou, Q. Li and Z. Peng, L. Wang, *Surf. Coat. Technol.*, 304 (2016) 179.
2. T.S.N. Sankara Narayanan, I.S. Park and M.H. Lee, *Prog. Mater. Sci.*, 60 (2014) 1.
3. M.K. Kulekci, *Int. J. Adv. Manuf. Technol.* 39 (2008) 851.
4. K. Ria and S.D. Choi, *J. Korean Phys. Soc.*, 54 (2009) 2409.
5. J. Zhang and C. Wu, *Corros. Sci.*, 2 (2010) 55.
6. Y. Pan, G. Wu, X. Cheng, Z. Zhang, M. Li, S. Ji and Z. Huang, *Corros. Sci.*, 98 (2015) 672.
7. R.C. Zeng, L. Sun, Y.F. Zheng, H.Z. Cui and E.H. Han, *Corros. Sci.*, 79 (2014) 69.
8. Z. Li, Y. Yuan, P. Sun and X. Jing, *Appl. Mater. Interfaces*, 3 (2011) 3682.
9. J.E. Gray and B. Luan, *J. Alloys Compd.*, 336 (2002) 88.
10. W.R. Zhou, Y.F. Zheng, M.A. Leeftang and J. Zhou, *Acta Biomater.*, 9 (2013) 8488.
11. N. Yamauchi, N. Ueda, A. Okamoto, T. Sone, M. Tsujikawa and S. Oki, *Surf. Coat. Technol.*, 201 (2007) 4913.
12. Y. Son, D. Shan, R. Chen, F. Zhang and E.H. Han, *Surf. Coat. Technol.*, 203 (2009) 1107.

13. K. Dong, Y. Song, D. Shan and E.H. Han, *Surf. Coat. Technol.*, 266 (2015) 188.
14. A. Lugovskoy and M. Zinigrad, *Materials Science - Advanced Topics*, InTech, (2013).
15. L.H. Li, T.S.N. Sankara Narayanan, Y.K. Kim, J.Y. Kang, I.S. Park, T.S. Baea and M.H. Lee, *Surf. Interface Anal.*, 46 (2014) 7.
16. A. Nominé, J. Martin, G. Henrion and T. Belmonte, *Surf. Coat. Technol.*, 269 (2015) 131.
17. J. Liang, L. Hu and J. Hao, *Appl. Surf. Sci.*, 253 (2007) 6939.
18. S. Durdu and M. Usta, *Appl. Surf. Sci.*, 261 (2012) 774.
19. R.O. Hussein, X. Nie and D.O. Northwood, *Electrochim. Acta.*, 112 (2013) 111.
20. R.O. Hussein, P. Zhang, X. Nie, Y. Xia and D.O. Northwood, *Surf. Coat. Technol.*, 206 (2011) 1990.
21. S.J. Lee and L.H.T Do, *Surf. Coat. Technol.*, 307 (2016) 781.
22. R.F. Zhang, D.Y. Shan, R.S. Chen and E.H. Han, *Mater. Chem. Phys.*, 107 (2008) 356.
23. L.R. Chang, F.H. Cao, J.S. Cai, W.J. Liu, Z. Zhang and J.G. Zhang, *Trans. Nonferrous Met. Soc. China*, 21 (2011) 307.
24. Y. Yang and H. Wu, *Trans. Nonferrous Met. Soc. China.*, 20 (2010) s688.
25. O. Khaselev, D. Weiss and J. Yahalom, *Corros. Sci.*, 43 (2001) 1295.
26. G.H. Lv, H. Chen, W.C. Gu, L. Li, E.W. Niu and X.H. Zhang, *J. Mater. Process. Tech.*, 208 (2008) 9.
27. I.J. Hwang, D.Y. Hwang, Y.G. Ko and D.H. Shin, *Surf. Coat. Technol.*, 206 (2012) 3360.
28. Y. Gu, S. Bandopadhyay, C.F. Chen, Y. Guo and C. Ning, *J. Alloys Compd.*, 543 (2012) 109.
29. X. Yongjun, *Curr. Appl. Phys.*, 10 (2010) 719.
30. Z.J. Li, Y. Yuan and X.Y. Jing, *Mater. Corros.*, 65 (2014) 493.
31. C. Wang, B. Jiang, M. Liu and Y. Ge, *J. Alloys Compd.*, 621 (2015) 53.
32. X. Lu, C. Blawert, M. Mohedano, N. Scharnagl, M.L. Zheludkevich and K.U. Kainer, *Surf. Coat. Technol.*, 289 (2016) 179.
33. Z. Qiu, R. Wang, X. Wu and Y. Zhang, *Int. Electrochem. Sci.*, 8 (2013) 1957.
34. Y. Ma, X. Nie, D. Northwood and H. Hu, *Thin Solid Films*, 494 (2006) 296.
35. L.L. Liu, P.X. Yang, C.N. Su, H.F. Guo and M.Z. An, *Int. Electrochem. Sci.*, 8 (2013) 6077.
36. S. Wu, Y. Zhang, Z. Wei, Y. Sheng, X. Zhou and Q. Chen, *Int. Electrochem. Sci.*, 9 (2014) 4394.
37. Y.K. Lee, K. Lee and T. Jung, *Electrochem. Commun.*, 10 (2008) 1716.
38. B. Zou, G.H. Lu, G.L. Zhang and Y.Y. Tian, *Trans. Nonferrous Met. Soc. China*, 25 (2015) 1500.